

Simulations of Large-Scale Zero Boiloff, Densification, and Solidification of Hydrogen

Colin P. Mahony¹

University of Memphis, Memphis, Tennessee, 38111, United States

Jeffrey G. Marchetta²

University of Memphis, Memphis, Tennessee, 38111, United States

and

Adam M. Swanger³

NASA Kennedy Space Center, Cryogenics Test Laboratory, KSC, Florida, 32899, United States

Abstract

An Integrated Refrigeration and Storage (IRAS) experimental system called the Ground Operations and Demonstration Unit for Liquid Hydrogen (GODU-LH2) demonstrated the ability to store cryogenics in a zero boiloff (ZBO) process, and to densify liquid hydrogen by reducing the temperature and pressure down to the triple point resulting in solidification. The incompressible Navier-Stokes was utilized to simulate ZBO, densification, and solidification of liquid hydrogen (LH2) in the IRAS tank. The simulations were performed using a commercially available Computational Fluid Dynamics (CFD) pressure-based mass and momentum flow model and an enthalpy-porosity energy model. Results demonstrated the simulation's ability to predict time-dependent flow and temperature fields and solid-liquid phase locations for hydrogen during ZBO, densification, and solidification. The simulations showed good agreement with experimental data, with errors within acceptable ranges for temperature and pressure predictions, provided detailed insights into natural convection and solid-liquid phase change dynamics. These findings are critical for the design of future cryogenic fluid management systems.

1.0 Introduction

The space industry continues to utilize cryogenic liquids as the main propellants for launch vehicles and will likely rely on cryogenic propulsion systems for future long duration, human crewed space missions. One of the leading issues in the field of cryogenics is the efficient storage and transportation of cryogenic commodities [1]. Cryogenic liquids are normally stored at/near normal boiling point (NBP)—saturated at or near atmospheric pressure—in well-insulated tanks; and for hydrogen, the NBP is at a temperature of 20.27 K. Being stored in this saturated state, any

¹ Graduate Research Assistant, Department of Mechanical Engineering.

² Professor, Department of Mechanical Engineering.

³ Principal Investigator, Cryogenics Test Laboratory.

heat leak into the tank would contribute to liquid loss due to boiloff [2]. Controlling the heat transfer into cryogenic storage vessels has been the motivation for numerous research projects.

To store cryogenics for longer periods, the heat transfer into the tank must be controlled passively with insulations and/or actively via refrigeration. Key developments in ZBO technologies have focused both passive methods, such as multilayer insulation (MLI) and vapor-cooled shields, and active approaches, which incorporate refrigeration systems to actively counteract heat ingress. Passive methods rely on improved insulation materials to minimize external heat loads, while active methods employ external power to remove heat via cryogenic refrigerators and cryocoolers. Examples of active cooling technologies include the reverse Turbo-Brayton cycle, Stirling, and Pulse-Tube coolers. Hybrid ZBO systems that integrate both passive and active technologies have proven particularly effective in reducing boiloff losses, enabling densification, and maintaining cryogenic fluids over long durations. These systems combine passive insulation layers, such as MLI, with active cooling components to intercept and reject heat leaks, ensuring robust temperature and pressure control [3-8].

One of the hybrid methods of controlling the heat leak into a cryogenic vessel from the environment is called Integrated Refrigeration and Storage (IRAS). The IRAS technology couples a storage vessel with an internal heat exchanger distributed throughout the tank volume connected to an external cryogenic refrigeration system [1,4-5]. Unlike conventional tanks, IRAS systems amplify natural convection near refrigeration coils due to localized temperature gradients. These amplified convection currents create localized cooling zones that enhance heat transfer and influence both stratification and phase transitions. In IRAS tanks, this interaction between the refrigeration system and natural convection allows for efficient thermal management, enabling processes such as densification and solidification that are not achievable in conventional tanks. The refrigeration coils' geometry also induces unique flow patterns that optimize localized cooling while maintaining bulk fluid stability. In contrast, conventional tanks primarily rely on passive insulation to minimize boiloff, with less emphasis on actively influencing fluid dynamics or phase transitions. While natural convection still occurs due to external heat transfer, the lack of localized cooling sources limits its impact compared to active systems like IRAS [9].

Depending on the capacity of the refrigerator, the system could achieve ZBO, in-situ liquefaction, or conditioning/densification of the cryogenic fluid. If the capacity of the refrigerator matches the heat leak, then ZBO is achieved, and if the capacity exceeds the heat leak, then

densification occurs. An IRAS system allows the liquid to be stored in a quasi-equilibrium state, and the ability to cool the liquid directly, via free convection, allows for control of the bulk temperature of the fluid. This also enables manageable depressurization of tank ullage pressure and bulk fluid conditioning for greater system control [3-4, 6, 8].

The Ground Operations and Demonstration Unit for Liquid Hydrogen (GODU-LH2) proved the ability to achieve ZBO and to densify hydrogen on a large-scale and at multiple fill levels [7]. The experimental IRAS tank at the Cryogenics Test Laboratory (CTL) at KSC also demonstrated zero loss tank chill down from ambient temperature and zero loss tanker off-loading of the LH₂. During the densification testing, this system brought the temperature and pressure down to the triple point and below, suggesting solidification of hydrogen on in a large-scale cryogenic tank [6]. The GODU-LH2 confirmed the ability to control a full-scale LH₂ tank, however the influence of free convection on ZBO and densification was not fully resolved since the flow inside the tank could not be visualized. In addition, the solidification of the hydrogen adjacent to the refrigeration coils inside the tank could not be observed directly [5-7].

Numerous thermodynamic models have also been developed to reliably predict tank pressure and bulk temperature of cryogenic fluids during cryogenic boiloff, ZBO, and densification [4,10-12]. Commercially available CFD models have been validated to simulate fluid flow, heat transfer, and phase change for a wide variety of applications. Stewart et al. demonstrated the use of ANSYS Fluent in simulating self-pressurization of cryogenic hydrogen tanks, providing insights into natural convection, phase interactions, and the sensitivity of pressure evolution to initial temperature distributions [13]. Additionally, studies by Molkov et al., Kassemi et al., and Kartuzova et al. demonstrated the effectiveness of pressure-based solvers in ANSYS Fluent for modeling hydrogen flow and heat transfer under various cryogenic conditions. These studies highlight the robustness of Fluent for capturing buoyancy-driven natural convection and stratification in cryogenic systems [14-16].

Additionally, Alam et al. validated the use of the enthalpy-porosity method for simulating solidification and melting in phase change materials embedded in heat exchangers. Their study demonstrated the solver's accuracy, with temperature deviations of less than 2 K when compared to experimental results. While their work focused on PCMs rather than cryogenic fluids, it provides critical validation for the numerical methods employed in this study [17]. However, the effects of

heat transfer due to natural convection on the fluid flow and solidification of LH2 in large scale tanks, such as the IRAS tank, have not been studied in detail.

This study expands upon prior research by employing commercial CFD software with validated physical models to simulate the ZBO, densification, and solidification phases of the GODU-LH2 IRAS experiments, specifically addressing the challenges unique to cryogenic applications. To date, experiments in large scale tanks have focused on collecting data for global fluid and flow properties rather than attempting to visualize the transient flow field, temperature field, and phase location. By employing high-fidelity CFD methods, this research aims to enhance the understanding of natural convection, phase transitions, and solidification processes in large scale cryogenic storage tanks by simulating highly resolved, transient flow fields, temperatures, and solid-liquid phase locations. The CFD simulation results are compared to experimental data to assess the accuracy of CFD model. In addition, the results provide valuable insights that have not previously been observed experimentally in a large-scale hydrogen tank. An accurate CFD model can subsequently be used in future work to design and optimize advanced cryogenic systems.

2.0 GODU-LH2 Experimental Setup

The GODU-LH2 vacuum-jacketed tank can safely store up to 125,000 L of LH2 at NBP, corresponding to a “100% full” tank. According to the experiment investigators, a “100% fill” represents a liquid volume equal to 90% of the total tank capacity, with the remaining 10% allotted for ullage. The outer jacket measures approximately 23 m in length and 3.4 m in diameter, while the inner tank dimensions are 21.8 m long and 2.9 m in diameter.

The internal helium refrigerant IRAS heat exchanger consists of nearly 290 m of stainless-steel tubing, featuring two upper and lower 25 mm manifolds and forty evenly spaced 6.4 mm diameter tubes, bent into a 3-dimensional shape that follows the tank wall's curvature. The closed-loop helium refrigeration system, distributed throughout the storage tank volume, enables effective conditioning of the entire bulk cryogenic liquid. The helium heat exchanger manifolds and coils provide a total heat transfer area of approximately 8 m².

Twenty-four silicon diode temperature sensors are employed inside the tank: twenty (TT1-TT20) distributed along three rakes, and four (TT21-TT24) positioned at the inlet and exit of two 6.4 mm coils, measuring the helium temperature. The diodes are calibrated ± 0.5 K from 450 K to 25 K and ± 0.1 K from 25 K to 1.5 K. Fig 1 presents a diagram of the GODU-LH2 tank which includes the IRAS modifications. Fig 2 shows the location of the diodes relative to the approximate

position of the liquid-vapor interface for both fill levels, as visualized based on experimental data. Table 1 shows the position of diodes TT1 through TT20 inside the tank [1, 5-7,11].

The liquid levels for the 100% and 67% fill cases were determined using a differential pressure sensor. This sensor measured the hydrostatic pressure difference between the liquid and ullage regions, providing precise volumetric data for each fill level. While the diodes (TT1-TT20) were strategically placed to monitor temperature profiles and stratification within the tank, they were not employed to measure liquid levels. Figure 2 provides an approximate visualization of the 67% and 100% liquid levels based on experimental data and the tank's geometry.

The temperature and pressure measurements obtained during the 100% and 67% fill level experiments are presented in Fig 3 a) and b), and also illustrates the types of experiments conducted at both the fill levels. The liquid was off loaded during the tanker off load portion, and then the boiloff testing began. Several ZBO tests were conducted, utilizing three distinct control methods: Duty Cycling (ZBO-DC), Pressure-Controlled (ZBO-PC), and Temperature-Controlled (ZBO-TC). In the ZBO-DC tests, the helium refrigerator was cycled on and off at full power, creating temperature and pressure oscillations in the IRAS tank. During the ZBO-PC phase, the helium refrigerator's operation was regulated by the tank pressure sensor. If the tank pressure increased above a specified set point, the refrigerator adjusted its cooling capacity to maintain the desired pressure. In the ZBO-TC phase, the helium refrigerant temperature was directly controlled using a refrigerator command and software interface, maintaining the helium supply temperature at a constant value. The final portion of the experiments consists of the densification phase, which also includes solidification when the LH₂ reached the triple point. The 100% fill experiment was cut short before the triple point was reached due to the impending project close-out, coupled with a shut-down caused by hurricane Matthew that made landfall at KSC in October 2016; however, the 67% fill test was maintained at the triple point for approximately 30 hours which suggests that's a portion of the LH₂ solidified.

As previously mentioned, diodes TT21 – TT24 were inserted in the helium flow stream at the top and bottom of two heat exchanger coils to gather the temperature of the helium refrigerant inlet and outlet of the coils. Pressure transducers, or PT 2, were used to measure the tank pressure. Table 2 shows the average heat loads and heat fluxes for both fill levels, which can be calculated using an average of the measured boiloff flow rate, tank pressure, and temperature differences [11]. The outer wall boundary conditions were based on the calculated values in Table 2.

3.0 Model Development

3.1 Model Setup

The finite volume software employed for simulating the quasi-steady ZBO, densification, and solidification phases of the GODU-LH2 IRAS experiments is capable of solving the transient continuity, momentum, and energy equations. The software models fluid flow, heat transfer, and solidification/melting phase change. The Boussinesq approximation is applied as a source term in the momentum equation to model natural convection, as density variations in cryogenic hydrogen due to temperature gradients are small and primarily influence buoyancy forces. This approximation has been validated in cryogenic applications, where buoyancy-driven flow plays a critical role in the dynamics of hydrogen storage tanks [16-18]. These studies demonstrate that the Boussinesq approximation effectively captures natural convection phenomena while maintaining computational efficiency in cryogenic systems.

The pressure-based solver uses the semi-implicit method for pressure-linked equations (SIMPLE) to calculate velocity and pressure sequentially. The model implements the pressure staggered option (PRESTO) for pressure, second-order upwind differencing for momentum and energy, and first-order implicit transient formulation for time. The linearized set of transport equations are solved using the algebraic multigrid (AMG) method. To model solidification, the enthalpy-porosity formulation is employed [19]. This method accurately models mushy zone phase-change problems and has been validated in various applications, including studies on embedded heat exchangers and phase change materials, demonstrating strong agreement between experimental and numerical results [17]. All simulations enforce a global residual tolerance of 1×10^{-6} .

The Navier-Stokes equations with an enthalpy formulation of the energy equation for a two-phase system can be written as

$$\nabla \cdot \vec{v} = 0 \quad (1)$$

$$\rho_o \left(\partial v_x / \partial t + \nabla \cdot (\vec{v} v_x) \right) = -\partial P / \partial x + \mu (\nabla \cdot (\nabla v_x)) + S_x \quad (2)$$

$$\rho_o \left(\partial v_y / \partial t + \nabla \cdot (\vec{v} v_y) \right) = -\partial P / \partial y + \mu (\nabla \cdot (\nabla v_y)) - g(\rho - \rho_o) + S_y \quad (3)$$

$$\rho_o \left(\partial v_z / \partial t + \nabla \cdot (\vec{v} v_z) \right) = -\partial P / \partial z + \mu (\nabla \cdot (\nabla v_z)) + S_z \quad (4)$$

The enthalpy, h , form of the energy equation is:

$$\rho_o \left(\partial h / \partial t + \nabla \cdot (\vec{v} h) \right) = \partial P / \partial t - \nabla \cdot (k \nabla T) - \Delta H d\beta / dt \quad (5)$$

The lever rule is applied to determine the liquid fraction, β , as follows

$$\beta = \begin{cases} 0, & T < T_{solidus} \\ \frac{T - T_{solidus}}{T_{liquidus} - T_{solidus}}, & T_{solidus} < T < T_{liquidus} \\ 1, & T_{liquidus} < T \end{cases} \quad (6)$$

where P is the pressure, v is velocity, T is temperature, k is thermal conductivity, ρ is the density, ρ_0 is the reference density, ΔH is the latent heat, μ is absolute viscosity, and S is a momentum source term [19-20]. A Boussinesq approximation assumes the density differences in all the terms in the governing equations are negligible except the gravity term. As such the Boussinesq approximation is applied in the direction of gravity (i.e. the y momentum equation) where ρ_0 represented the reference density, g was the gravitational force, and ρ is the density. The enthalpy formulation of the phase change energy equation requires a Liquid Fraction, β . The Liquid fraction is the ratio of liquid to solid in a computational cell and is defined by a temperature window. While the computational cell is within the temperature window, between liquidus and solidus temperature, the cell is in a mushy zone. Then the source terms applied to the x-, y-, and z-momentum equations utilize the Enthalpy Porosity of flow through a porous material and were given as:

$$S_x = -C \frac{(1-\beta)^2}{\beta^3+0.001} v_x \quad (7)$$

$$S_y = -C \frac{(1-\beta)^2}{\beta^3+0.001} v_y \quad (8)$$

$$S_z = -C \frac{(1-\beta)^2}{\beta^3+0.001} v_z \quad (9)$$

where C is the mushy zone constant, 1×10^8 . As the cell solidifies or as the phase fraction goes to zero, the source term becomes larger which effectively reduces the velocities in the cell. Once the fluid in the cell is completely solidified, the source term is maximized, and the velocities go to zero [19].

The intensity of a buoyancy-driven flow is characterized using the Rayleigh number and the transition from laminar to turbulent flow begins when the Rayleigh number is greater than 1×10^9 . All flows in the validation cases have a Rayleigh number less than 1×10^8 , thus a laminar flow model is used for the simulations.

The GODU-LH2 IRAS tank is one of the only large-scale tanks to accomplish LH₂ densification and solidification, that was also well instrumented. As shown in Fig 1, the asymmetric three-dimensional shape of the heat exchanger coil inside the tank repeats along the length of the cylindrical tank. Given the large size of the tank, the computational domain can be reduced in size

by using a three-dimensional segment of the tank, which includes one complete section of the asymmetric heat exchanger coil as shown in Fig 4 (a) and mesh examples in Fig 4 (b-c). The tradeoff for reducing the size of the computational domain is the inability to study the influence of the tank endcaps on the heat transfer and flow field. It is reasonable to assume that based on the 2:1 ratio of the length to the diameter, the influence of the endcaps is negligible in comparison to the cylindrical wall and heat exchanger coil in the centralized region of tank where the measurement instruments were positioned. In reference to Fig 4, the simulation is setup with no slip flow boundary conditions along the interior cylindrical tank wall and exterior surface of the heat exchanger coil. The two plane surfaces of the tank segment are specified as repeatable, permeable boundaries since the segment repeats along the length of the cylindrical tank.

The thermal boundary conditions for the inner tank wall are set to the constant heat flux values calculated in Table 2 for the two different fill levels. Thermal loads were calculated using average boiloff flow rates, tank pressure, and the log-mean temperature difference method to estimate heat fluxes at the tank boundaries. The initial temperature for the system was set at 25K for both the liquid and ullage domains. The hydrogen properties for the vapor, liquid, and solid phases used in the simulations were obtained from NIST [21]. All properties are assumed at saturation for all timesteps. The simulations assume there is no evaporation and condensation (i.e. no mass transfer between the liquid and the ullage). While it is expected that some LH2 will condense on the surfaces of the refrigeration coil in the ullage, the differential pressure measurements used to gauge the fill level during the experiment did not change significantly during the experiments once the tank was initially filled. This is expected due to the relatively small surface area of the coil compared to the large liquid hydrogen volume in the tank. This assumption also minimizes computational complexity without significantly affecting the bulk thermal or fluid dynamics under investigation. To simulate the quasi-steady portion of the ZBO-PC phase of the experiment, the refrigerant coil thermal boundary condition was specified to balance the total heat flux through the tank wall into the tank. The simulations are determined to be quasi-steady when the maximum computational cell temperature difference and velocity difference between timesteps is less than 1×10^{-6} . Using the experiment time as guidance, both fill level case simulations are set up for a physical runtime of 140 hours to reach a quasi-steady state. The simulations of densification phase are initialized with the final quasi-steady conditions. The same heat leak thermal boundary condition used for the quasi-steady simulations is specified for the densification cases. The heat

exchanger coil outer wall thermal boundary conditions for the refrigeration coil surface were derived from experimental temperature measurements (diodes TT21-TT24) and applied as heat flux values for ZBO and densification phases.

For both fill levels, simulations of the quasi-steady ZBO, densification, and solidification are performed using three different polyhedral unstructured, non-uniform meshes of increasing mesh density to assess the accuracy of the model such that the solution is in the asymptotic range of convergence. The 100% fill case is simulated using three meshes consisting of 200k, 350k, and 500k cells and the 67% fill case is simulated using three meshes consisting of 320k, 430k, and 660k, respectively. In both cases, the grid refinement ratio is greater than the minimum of 1.1 to allow the discretization error to be differentiated from other error sources [22]. The meshes are refined near the tank wall and refrigeration coil to resolve the regions of the temperature and velocity field where the gradients are expected to be more significant. The cell volume weighted formulation of the l_2 norm [23], shown in Equation 10, is utilized to compare the differences in the magnitude of the cell velocities between the unstructured, nonuniform meshes of increasing mesh density

$$l_2 = \sqrt{\frac{\sum_{i=1}^N ((v_{i,mesh1} - v_{i,mesh2})^2 * V_{i,mesh1})}{V_{tank}}} \quad (10)$$

Figs. 5-6 show a log-log plot of the l_2 norms as a function of the average cell size, h , comparing the simulation solution to the theoretical order of the mesh convergence, $\mathcal{O}(h^2)$.

4.0 Simulation Results

4.1 Zero Boiloff Results

After 120 hours of physical time, quasi-steady state solutions for both the 100% and 67% fill level cases are reached. Both simulations were extended for an additional 20 hours after meeting the aforementioned quasi-steady criteria to ensure the simulations remain at the quasi-steady condition and to match the time period of the experiments to enable comparison.

Fig 7 (a-d) presents a comparison of the temperature and pressure experiment measurements and the simulation predications for 20 hours of physical time. Fig 7 (a-b) shows that the quasi-steady LH₂ temperature is stratified in both fill level cases which is consistent with the experiment temperature measurements. The pressure for both of the ZBO cases remains constant over time as shown in Fig 7 (c-d).

Fig 8 (a) and (b) present the quasi-steady state temperature and velocity profiles for the 100%, and Fig 9 (a) and (b) shows 67% fill ZBO cases. The predictions show that the temperature of the LH₂ in both cases is stratified which is consistent with natural convection. For the velocity profiles presented in Fig 8 (b) and Fig 9 (b), the highest velocities in the computational domain occur in the ullage space for both cases which is due to the lower density of vapor relative to the liquid. The recirculation regions in the ullage and liquid are asymmetric along the x-y and y-z planes shown in Fig 8 (b) and Fig 9 (b) due to the asymmetry of the refrigeration coil. While not visible in Fig 8 (b) and Fig 9 (b), the recirculation zones are symmetric about the y-axis when viewed from a plane oriented 45° from the plane shown in Fig 8 (b) and Fig 9 (b). Although the velocity profiles in the liquid appear less differentiated than in the vapor due to the difference in velocity magnitudes, for the 100% fill level, the centralized recirculation zone in the 100% fill level cases can be discerned in Fig 8 (b).

4.2 Densification Results

Upon completion of the ZBO analysis, the densification simulations for both fill levels are initialized using the final temperature, pressure, and velocity predictions from the ZBO cases. The temperature and velocity profiles for the 100% fill densification case are presented in Fig 10 (a) and (b), while the simulation profiles for the 67% densification simulation shown in Fig 11 (a) and (b). Fig 12 (a) and (b) presented the results for the 100% fill level which has a shorter run time than the 67% fill since the refrigerator experienced issues the test was cut short for this case. Fig 13 (a) and (b) are the ullage temperature predictions and Fig 14 (a) and (b) show the pressure calculations compared to the experimental data. Densification for the 100% fill case ran for approximately 210 hours before the experimental data was stopped for the GODU-LH₂ tank, and TT3 did not function properly in this case and is omitted from the results. The 67% fill case ran for 360 hours such that the temperatures in several thermocouples dropped below the freezing temperature of hydrogen, which is 13.8 K, suggesting solidification occurred.

Fig 13 (a) and (b) present the ullage temperature profiles for the 100% and 67% fill densification cases. Similar to the ZBO cases, the densification temperature predictions show stratification, which is consistent with natural convection, while the refrigeration coil temperature is decreased. For the velocity profiles presented in Fig 10 (b) and Fig 11 (b), the velocities in both the liquid and ullage increase as the temperature of refrigeration coil due to the larger change in temperature across the computational domain. The recirculation regions in the ullage and liquid remain

asymmetric along the x-y and y-z planes shown in Figs 10 – 11 due to the asymmetry of the refrigeration coil.

4.3 Solidification Results

As mentioned previously, the LH₂ in the 100% fill case did not reach the triple point temperature of 13.8K and pressure of 7.04 kPa due to project close-out. Based on the LH₂ temperature (TT3-TT10) and pressure measurements shown in Fig 10 (b) and Fig 12 (b), respectively, the LH₂ in the 67% case reaches the triple point of hydrogen in the experiment after approximately 315 hours, which indicates that the liquid should begin solidifying. The tank pressure and local temperatures drop to the triple point and remain relatively constant through the end of this phase of the experiment.

The solidification simulation ran for approximately 50 hours and the transient data for the experiment is compared to the simulation results for the 660k mesh shown in Fig 15. The development of the solidified regions of hydrogen also results in a transient temperature and velocity profiles as shown in Figs 16(a – c) and Figs 17(a – c).

The experiment did not include any measurements or visualization of the solidified hydrogen, so the predictions of solidification represent the best attempt to visualize the solidified hydrogen in the tank. Given the accuracy of the simulation compared to temperatures and pressures measured, solidification can only be inferred. Fig 18 presents an isometric view of the solid phase front predictions in the computational domain over time. The isometric view is created using a 10 degrees rotation of the plane orthogonal to the outer tank wall. The enthalpy porosity model averages the properties of the fluid undergoing phase change in the mushy zone to minimize steep gradients. To visualize the edge of the phase-front, a choice must be made on a value of the phase fraction used in the visualization. To visualize the phase front, the contour shown in red in Fig 18 is for a solid phase fraction of 0.05 (i.e. 5% of the cell volume is solidified). The time sequence of images shows the predicted development of the solid phase front away from the surface of the refrigeration coil in the same direction as gravity. From Fig 18 (a), the solid hydrogen formation begins in the corners where the coils are close to the wall. Fig 18 (b) and (c) shows the formations at 15 hours and 50 hours after the onset of solidification. The development of the solid phase front is consistent with the natural convection driven recirculation flow of the LH₂ observed during ZBO and densification.

4.4 Discussion of Results

After reaching quasi-steady state, all the ZBO, densification, and solidification simulation predictions show quantitative agreement with the experimental data. Table 3 shows the maximum percent error analysis used to compare simulation predictions and the experimental results. As stated previously, simulation results are assumed to have achieved a reasonable level of mesh independence when the maximum percent error between the temperature predictions and the measurements are less than 10%. In all cases, mesh independence predictions are obtained using the 500k mesh for the 100% fill level case and the 660k mesh for the 67% fill level. With mesh independence established, the subsequent discussion only compares simulation predictions of the densest meshes, 500k for the 100% fill level and 660k for the 67% fill level.

The maximum percent error in temperatures for all simulations occurs in the ullage space at diode TT19. Table 3 shows the maximum percent error in temperatures and pressure for ZBO, densification, and solidification is less than 10% and 20%, respectively, for both fill levels. These low error values indicate a strong correlation between the simulation predictions and experimental data, validating the predictive accuracy of the model.

The observed stratified temperature profiles result from natural convection driven by buoyancy forces arising from temperature gradients. These forces create asymmetric recirculation zones in both the ullage and liquid phases, with stronger velocities in the ullage due to the lower density of the vapor. The asymmetric placement of the refrigeration coil amplifies these recirculation effects, resulting in localized cooling near the coil while slowing bulk fluid cooling in the liquid. During densification, as the refrigeration coil temperature decreases, the increasing temperature gradient intensifies natural convection. This leads to enhanced circulation within both the ullage and liquid spaces, redistributing heat more effectively. The simulation captures these dynamics accurately, as shown by the close agreement between predicted and experimental temperature and pressure profiles.

From the solidification analysis, the triple point temperature of hydrogen, 13.8 K, is reached in the 67% fill experiment. Following this, the experimental temperature drops below 13.8 K and remains relatively constant during the remainder of the solidification phase of the experiment. As mentioned previously, the 100% fill case did not reach the triple point temperature and pressure, so solidification was not observed. The fusion temperature for hydrogen is set at 13.8 K in the simulation, and the temperature predictions are consistent with this trend. The ratio of solid to

liquid in a computational cell, Liquid Fraction, shows the solid formation begins on the heat exchanger coils and progresses downward in the direction of gravity, consistent with natural convection-driven circulation of the LH2 inside the tank.

The simulation results provide a visualization of the solid phase front, with predictions showing the progression of solidification over time. For example, Fig. 18 illustrates how the solid hydrogen formation initiates in regions where the refrigeration coil is closest to the wall, progressing downward in a manner consistent with convection patterns observed during ZBO and densification phases. This progression underscores the critical role of localized cooling and buoyancy-driven flow in shaping the solid phase front. These findings collectively demonstrate the ability of the simulation to capture the physical mechanisms governing ZBO, densification, and solidification phases in cryogenic hydrogen tanks, providing valuable insights into the coupling of natural convection, thermal gradients, and phase change dynamics.

5.0 Conclusion

This study employed commercially available CFD software to simulate the ZBO, densification, and solidification phases of LH2 in the GODU-LH2 IRAS tank, demonstrating good agreement with experimental data. Quantitatively, the simulation results achieved maximum percent errors of less than 10% for temperature and less than 20% for pressure in all cases, validating the model's robustness and accuracy. These results were consistent across multiple mesh densities, with finer meshes providing marginally improved accuracy, particularly in the ullage space.

Key qualitative findings can be extracted from three-dimensional transient flow field and temperature field simulation results. The temperature stratification profiles driven by buoyancy forces are resolved as is the localized cooling near the refrigeration coil. The natural convection currents, amplified by the coil geometry, play a critical role in redistributing heat and stabilizing the bulk fluid. During the solidification phase, the predicted development of the solid phase front was consistent with natural convection-driven flow patterns, highlighting the coupling between thermal gradients and phase transitions in cryogenic systems.

The demonstrated ability of the simulation to model ground-based ZBO, densification, and solidification offers valuable tools for designing advanced cryogenic storage systems. Future work should focus on incorporating condensation effects in the ullage to further refine model accuracy and expanding the framework to include dynamic loading scenarios. By enhancing our

understanding of natural convection, stratification, and solidification, these findings contribute to optimizing cryogenic fluid management for aerospace and industrial applications.

References

- [1] Notardonato, W. U., Johnson, W. L., Swanger, A. M. and Tomsik, T. M., "Ground operations demonstration unit for liquid hydrogen initial test results," *Advances in Cryogenic Engineering, IOP Conf. Series: Materials Science and Engineering 101*, 2015.
- [2] Birmingham, B., Brown, E., Class, C. and Schmidt, A., "Vessels for the storage and transport of liquid hydrogen," *Journal of Research of the National Bureau of Standards*, 58(5), 1957, pp.243-253.
- [3] Hastings, L., Plachta, D., Salerno, L. and Kittel, P., "An overview of NASA efforts on zero boiloff storage of cryogenic propellants," *Cryogenics*, 41(11-12), 2001, pp.833- 839.
- [4] J.K. Partridge, J.W. Tuttle, W.U. Notardonato, W.L. Johnson., "Mathematical model and experimental results for cryogenic densification and sub-cooling using a submerged cooling source," *Cryogenics*, Volume 52, Issues 4–6, 2012, pp 262-267.
- [5] Notardonato, W., Swanger, A., Fesmire, J., Jumper, K., Johnson, W. and Tomsik, T., "Final test results for the ground operations demonstration unit for liquid hydrogen," *Cryogenics*, 88, 2017, pp.147-155.
- [6] Swanger, A. M., Notardonato, W. U., Fesmire, J. E., Jumper, K. M., Johnson, W. L. and Tomsik, T. M., "Large scale production of densified hydrogen to the triple point and below," *Advances in Cryogenic Engineering, IOP Conf. Series: Materials Science and Engineering 101*, 2017.
doi:10.1088/1757-899X/278/1/012013
- [7] Notardonato, W. U., Swanger, A. M., Fesmire, J. E., Jumper, K. M., Johnson, W. L. and Tomsik, T. M., "Zero boiloff methods for large scale liquid hydrogen tanks using integrated refrigeration and storage," *Advances in Cryogenic Engineering, IOP Conf. Series: Materials Science and Engineering 101*, 2017.
doi:10.1088/1757- 899X/278/1/012012
- [8] Plachta, D., Johnson, W. and Feller, J., "Zero boiloff system testing," *Cryogenics*, 74, 2016, pp.88-94.
- [9] Swanger, A. M., Notardonato, W. U., Johnson, W. L., and Tomsik, T. M., "Integrated Refrigeration and Storage for Advanced Liquid Hydrogen Operations". *19th International Cryocooler Conference Proceedings*, Vol.19, pp.513-522, 2016.
- [10] Al Ghafri, S.Z.S.; Swanger, A.; Jusko, V.; Siahvashi, A.; Perez, F.; Johns, M.L.; May, E.F., "Modelling of Liquid Hydrogen Boil-Off," *Energies*, Vol. 15, 2022, pp.1149.
doi:10.3390/en15031149
- [11] Swanger, Adam, "Large Scale Cryogenic Storage With Active Refrigeration", Electronic Theses and Dissertations. 6379. 2018. <https://stars.library.ucf.edu/etd/6379>
- [12] Yang, H. Q., Patel, C. S., Williams, B. R., "Validation of cryogenic propellant tank self-pressurization using Loci-Stream CFD tool," *NASA Technical Paper*, 2022, pp. 1-20.
- [13] Stewart, J. A., Moder, J. P., "Self-Pressurization of a Flightweight, Liquid Hydrogen Tank: Simulation and Comparison with Experiments," *52nd AIAA/SAE/ASEE Joint Propulsion Conference*, 2016.
- [14] Molkov, V., Ebne-Abbasi, H., Makarov, D., "Liquid hydrogen refuelling at HRS: Description of sLH2 concept, modelling approach and results of numerical simulations," *International Journal of Hydrogen Energy*, 2024, pp. 285-296.
- [15] Kassemi, M., Hauser, D., Kartuzova, O., Hylton, S., "CFD Model Development of a Cryogenic Storage Tank Self-Pressurization in Normal Gravity and Validation against SHIVER Experiment," *AIAA SciTech Conference Proceedings*, 2023.

- [16] Kartuzova, O., Kassemi, M., Hauser, D., "Development and Validation of Two-Phase CFD Models for Key Elements of Propellant Tank CFM Operations in 1G and Microgravity – An Overview," *AIAA SciTech Conference Proceedings*, 2023.
- [17] Alam, T.; Bacellar, D.; Ling, J.; and Aute, V., "Numerical Study And Validation Of Melting And Solidification In PCM Embedded Heat Exchangers With Straight Tube," *International Refrigeration and Air Conditioning Conference*, 2021.
- [18] Yang, H. Q., West, J., "CFD Extraction of Heat Transfer Coefficient in Cryogenic Propellant Tanks," *51st AIAA/SAE/ASEE Joint Propulsion Conference*, 2015.
- [19] V. R. Voller and C. Prakash, "A Fixed grid numerical modelling methodology for convection diffusion mushy region phase change problems," *International Journal Heat Mass Transfer*, vol. 30, no. 8, 1987, pp. 1709–1719.
- [20] ANSYS FLUENT 19.1 Theory Guide, 2021.
- [21] Lemmon, E., "Reference Fluid Thermodynamic and Transport Properties Database (REFPROP)," [online] NIST. URL: <https://www.nist.gov/programs-projects/reference-fluid-thermodynamic-and-transport-properties-database-refprop> [retrieved 5 Feb. 2022].
- [22] Roache, P.J., *Verification and Validation in Computational Science and Engineering*, Hermosa Publishers, Albuquerque, New Mexico, 1998.
- [23] Sun, M., Takayama, K., "Error localization in solution-adaptive grid", *Journal of Computational Physics*, Volume 190, pp. 346--350, 2003.

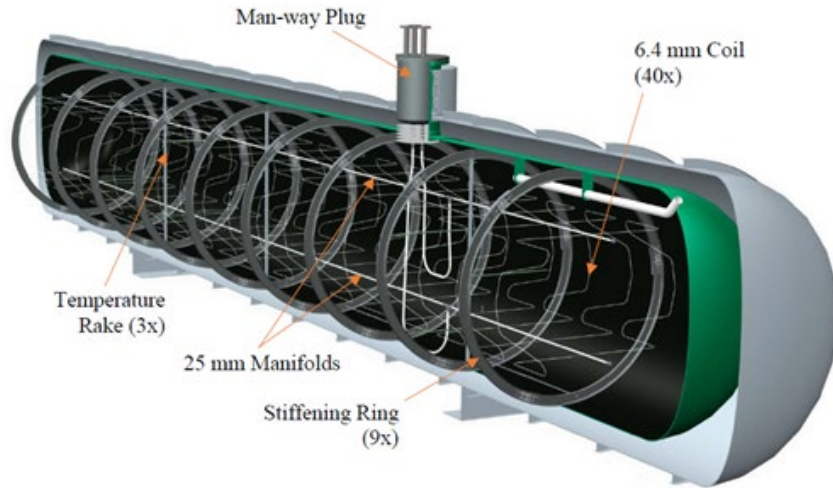


Fig. 1. Cut-away of GODU-LH2 with IRAS modifications

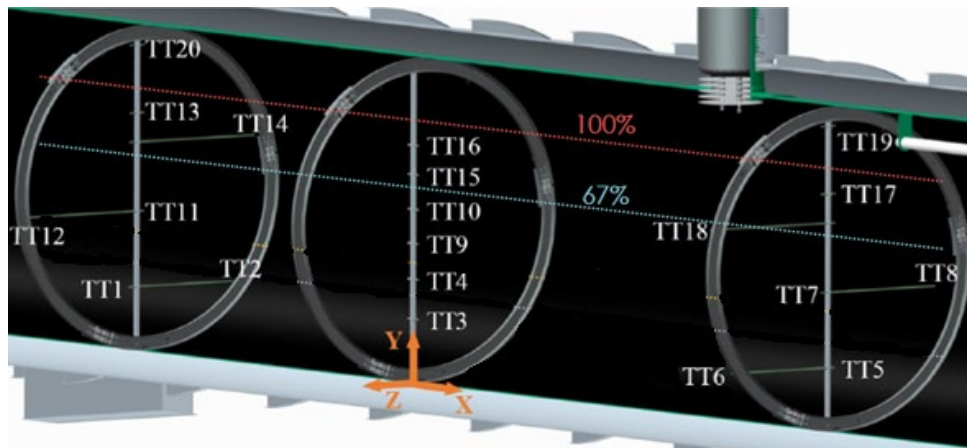
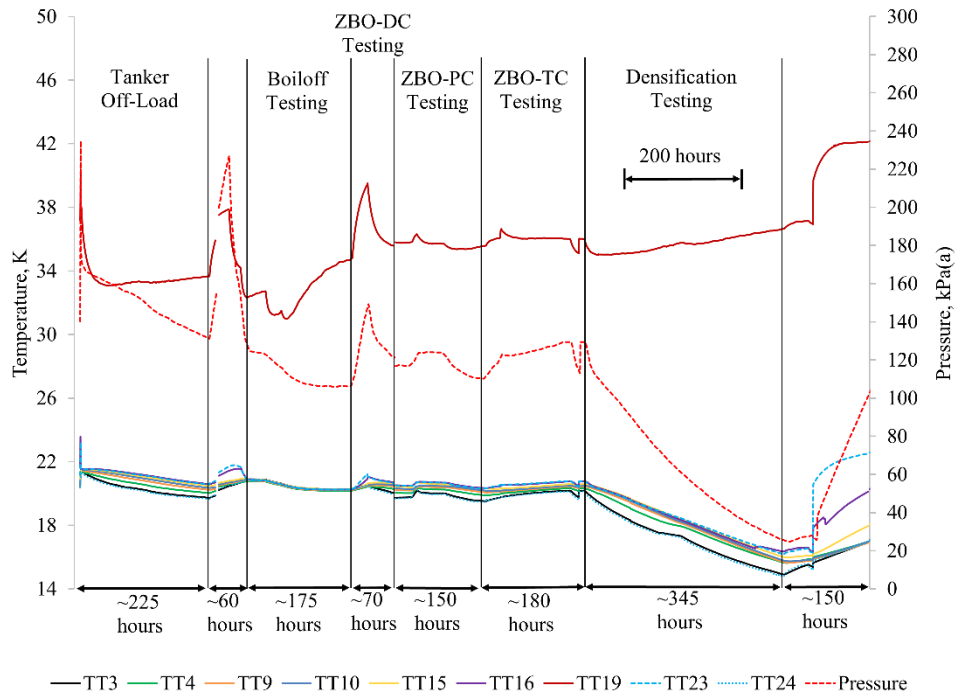
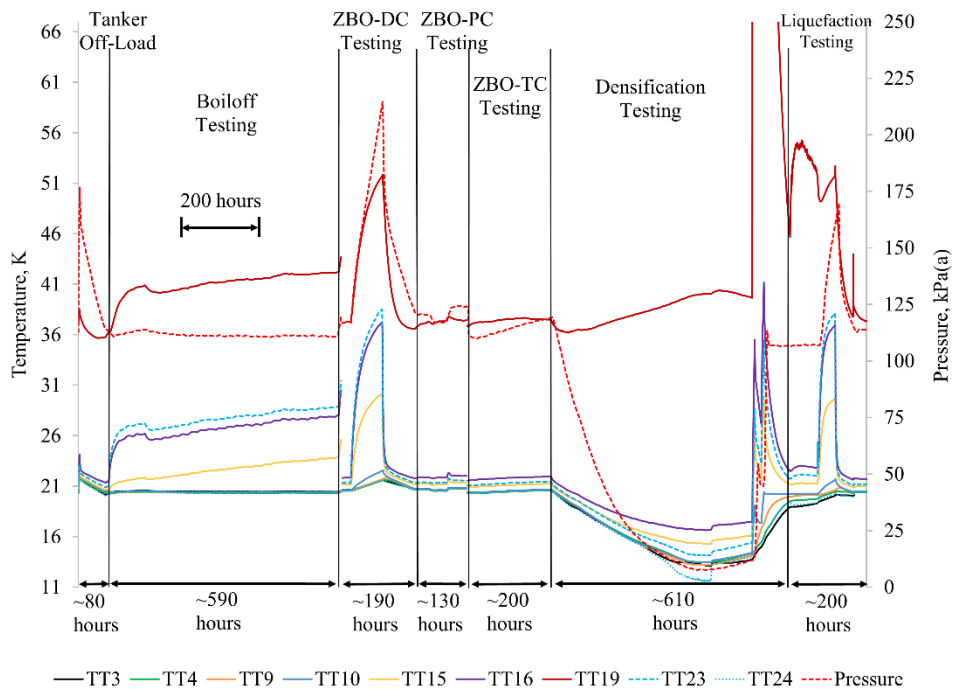


Fig. 2. Temperature rakes, diode positions, and fill levels

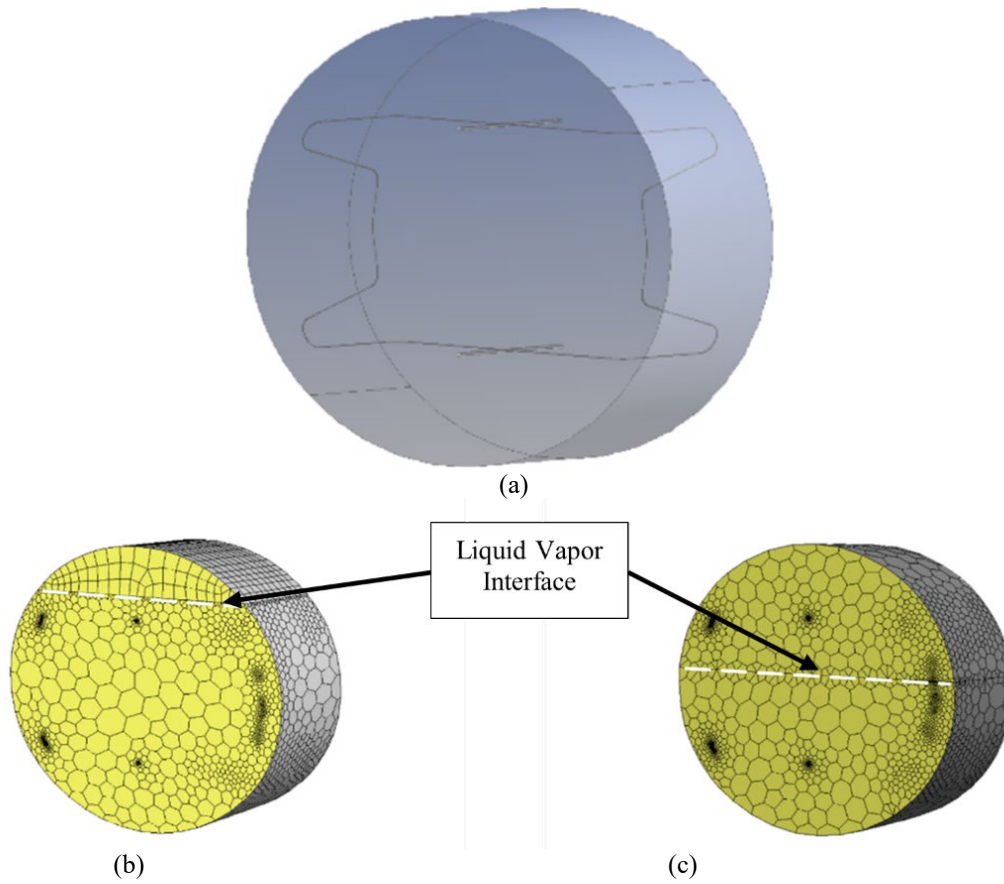


a)



b)

Fig. 3. Experimental temperatures and pressures for a) 100% fill and b) 67% fill



(b) (c)
Fig. 4. (a) Tank domain with single coil, (b) 100% fill mesh, (c) 67% fill mesh
(the dashed white line represents the position of the liquid-vapor interface for
reference)

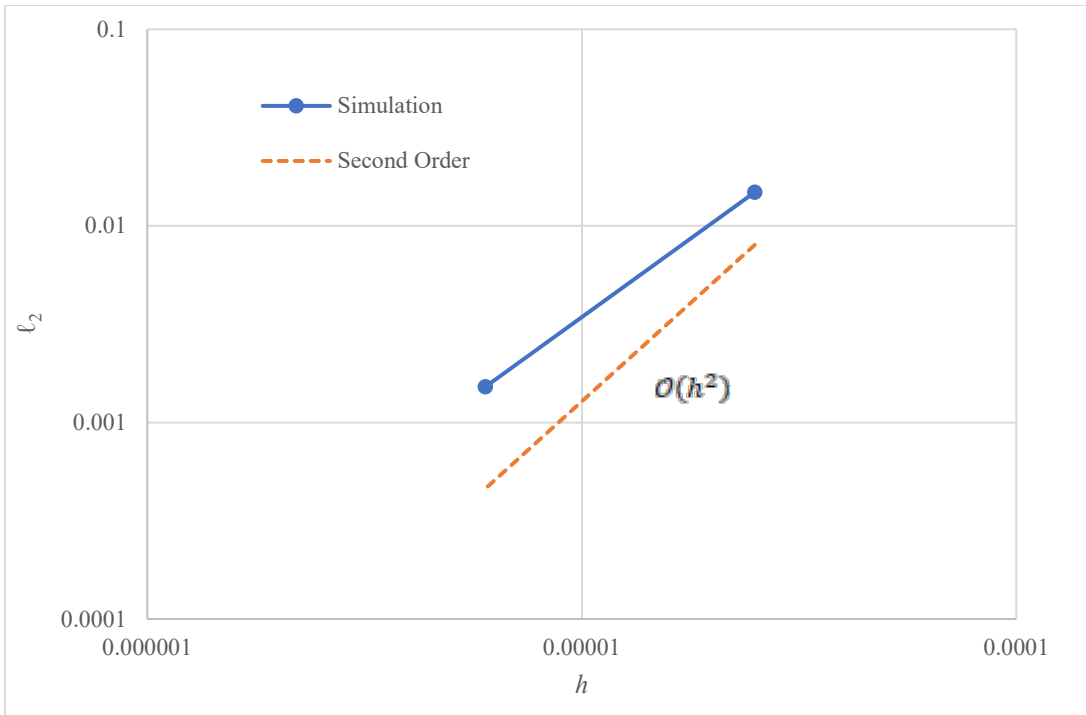


Fig. 5. l_2 norms for the 100% fill quasi-steady case

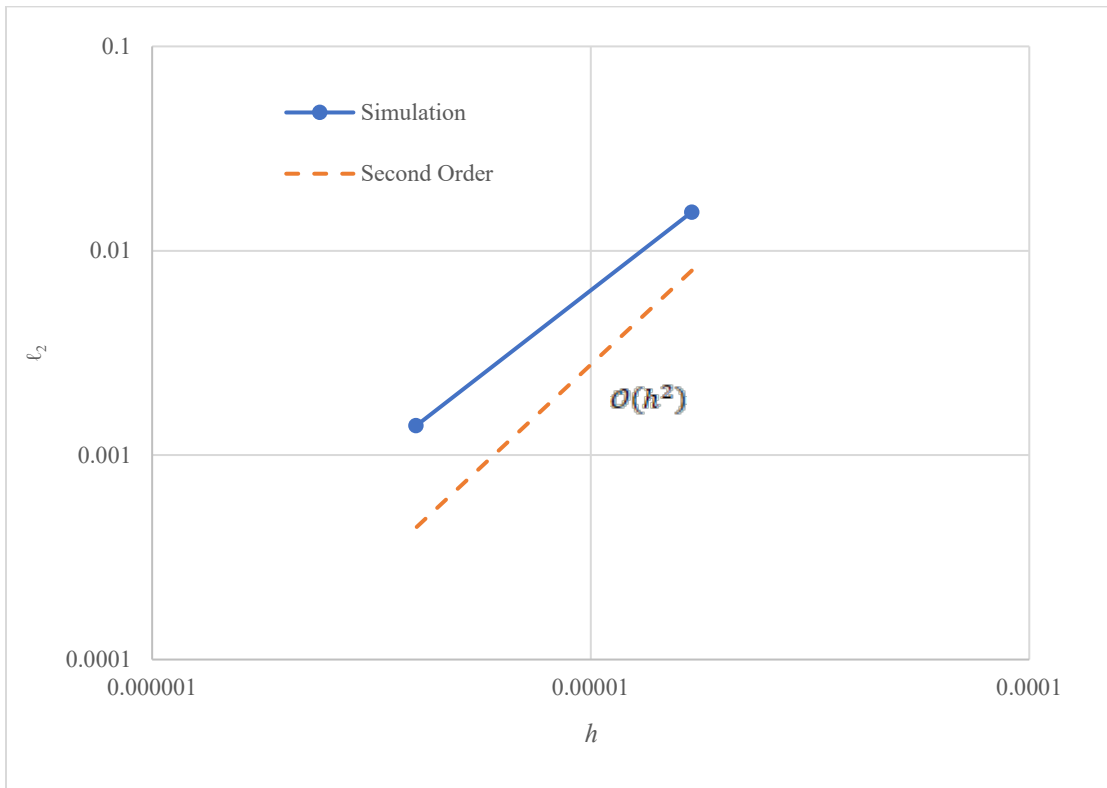
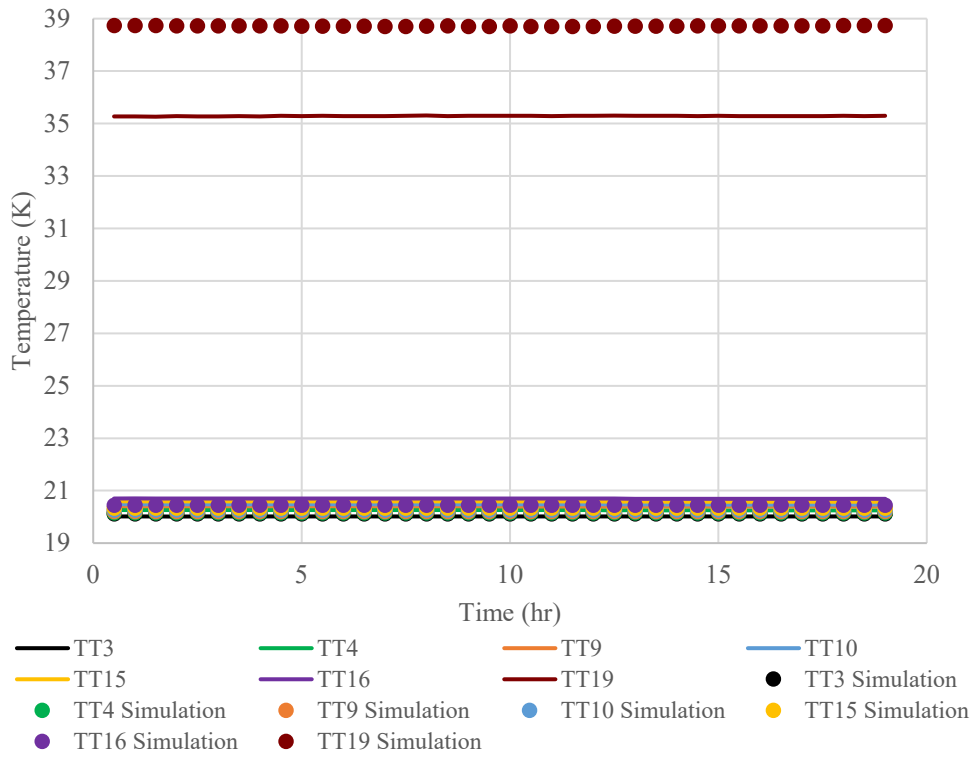
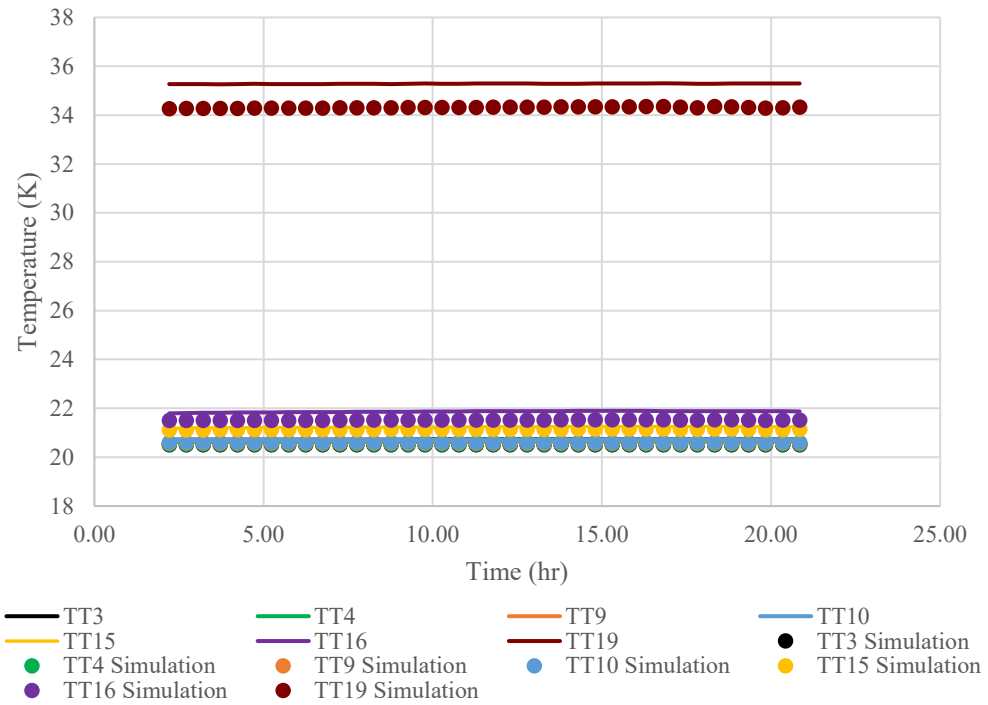


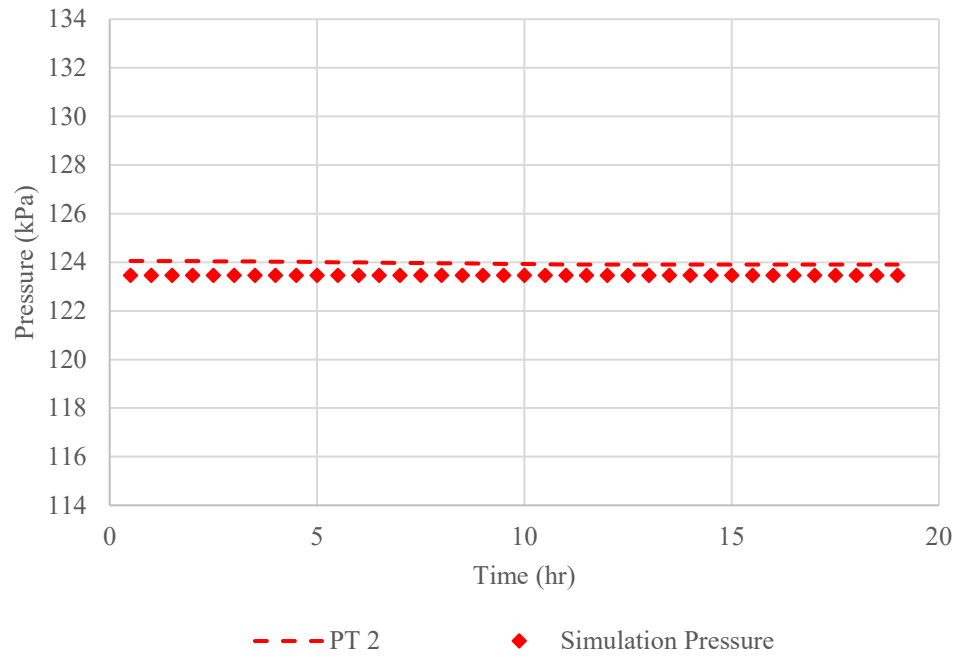
Fig. 6. l_2 norms for the 67% fill quasi-steady case



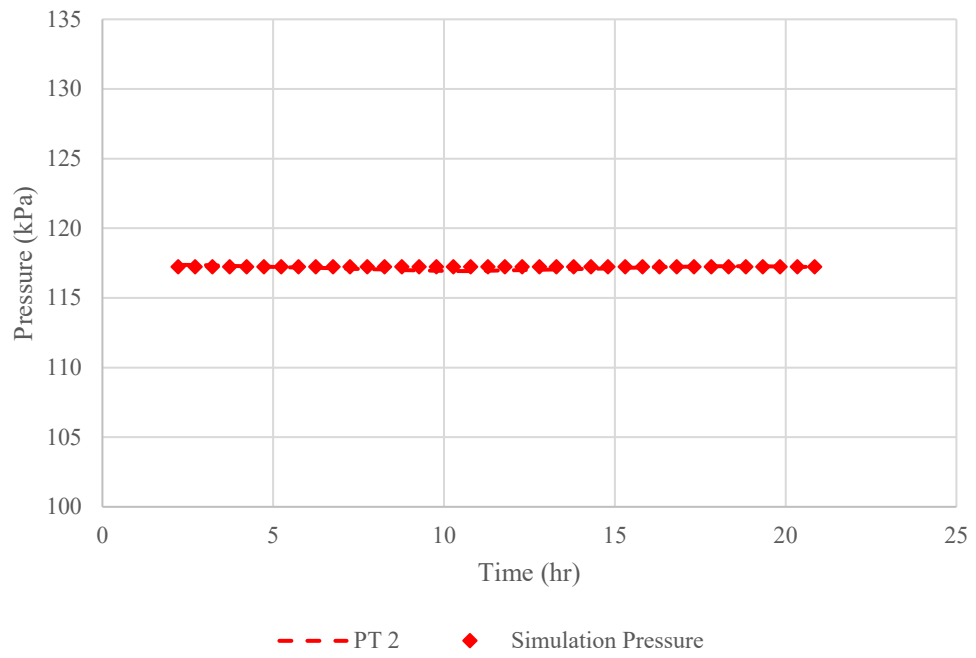
(a)



(b)



(c)



(d)

Fig. 7. ZBO temperature compared to experimental data for (a) 100% fill and (b) 67% fill;
ZBO pressure compared to experimental data for (c) 100% fill and (d) 67% fill

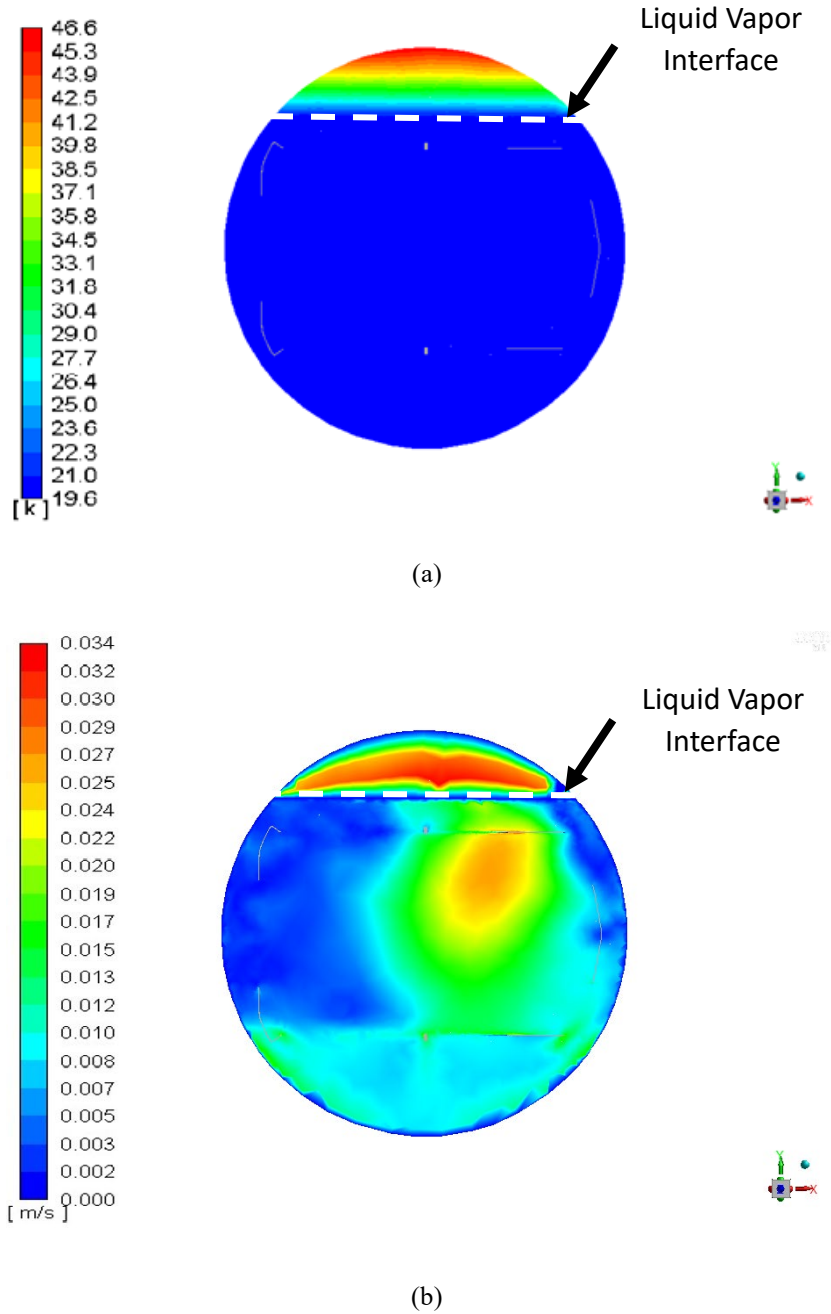
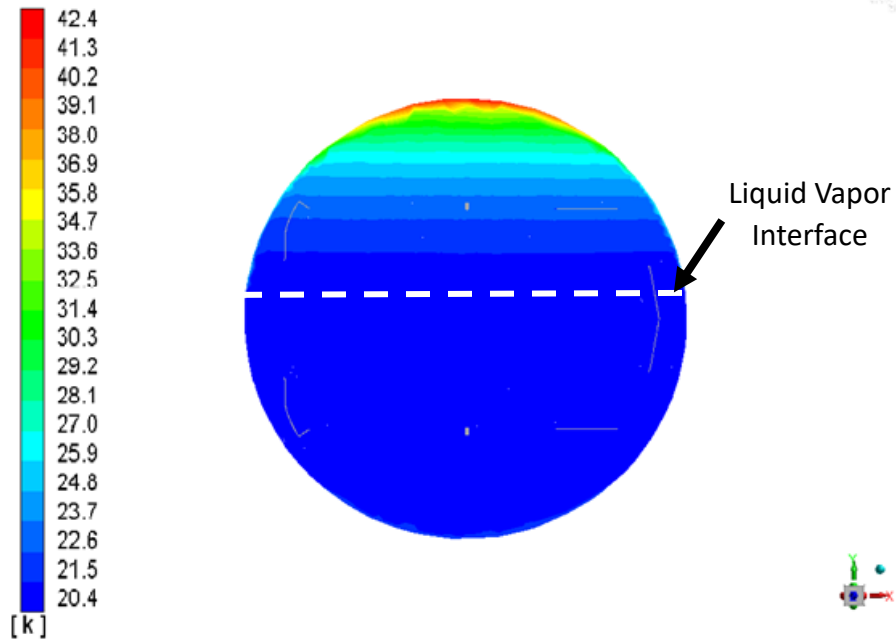
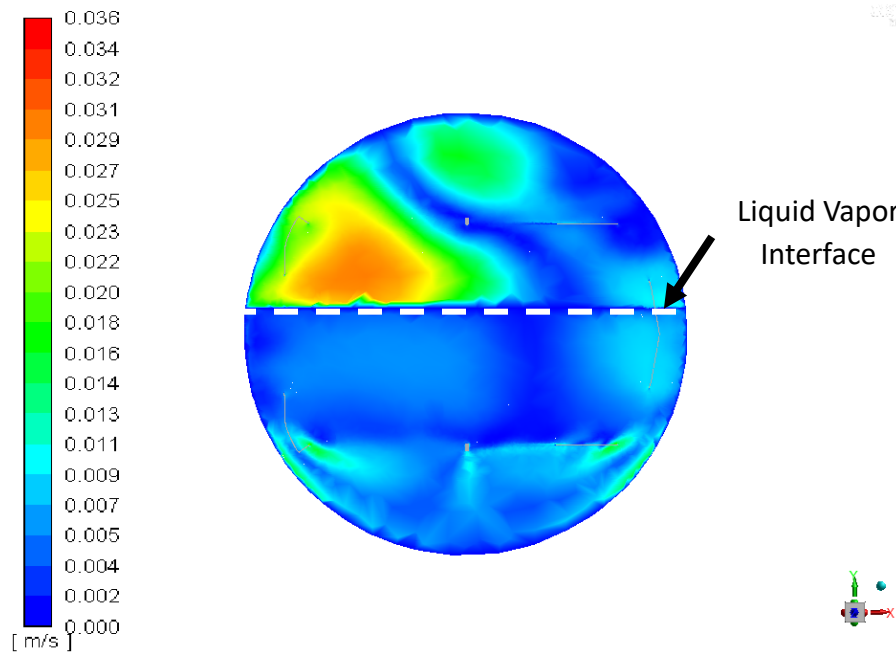


Fig. 8. ZBO 100% fill with liquid vapor interface: (a) Temperature profile, and (b) Velocity profile at time = 120 hours

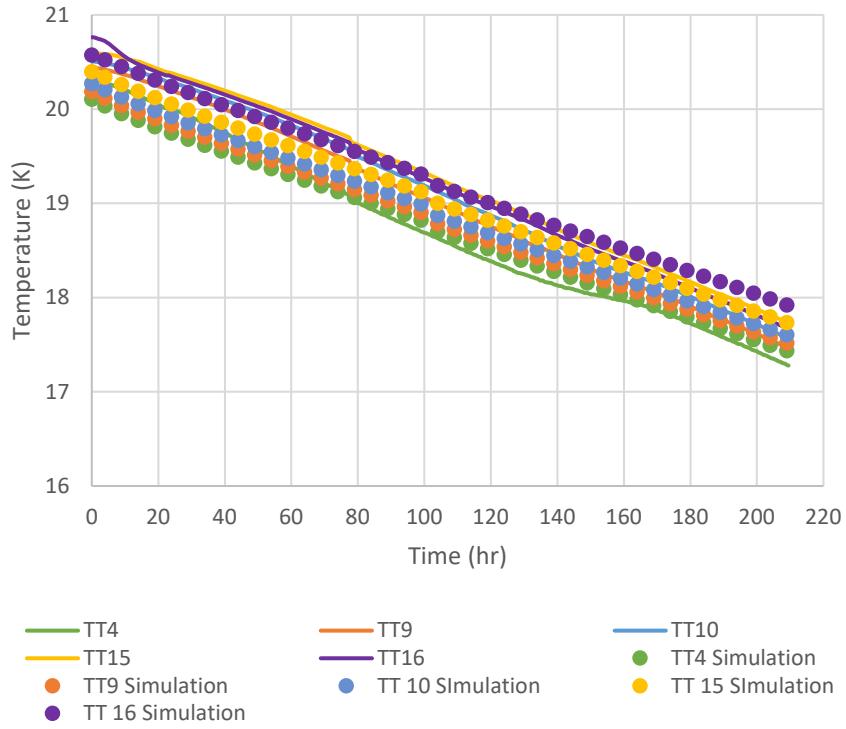


(a)

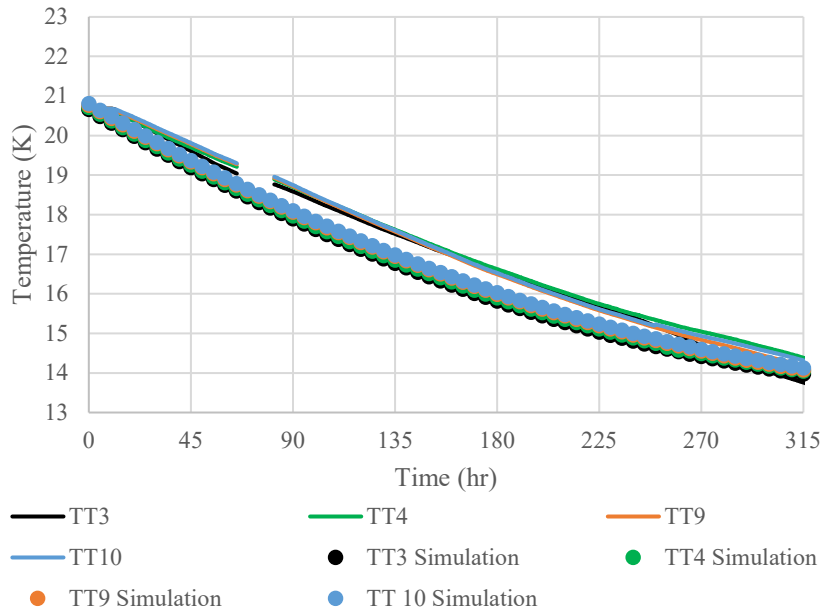


(b)

Fig. 9. ZBO 67% fill with liquid vapor interface: (a) Temperature profile, and (b) Velocity profile at time = 120 hours



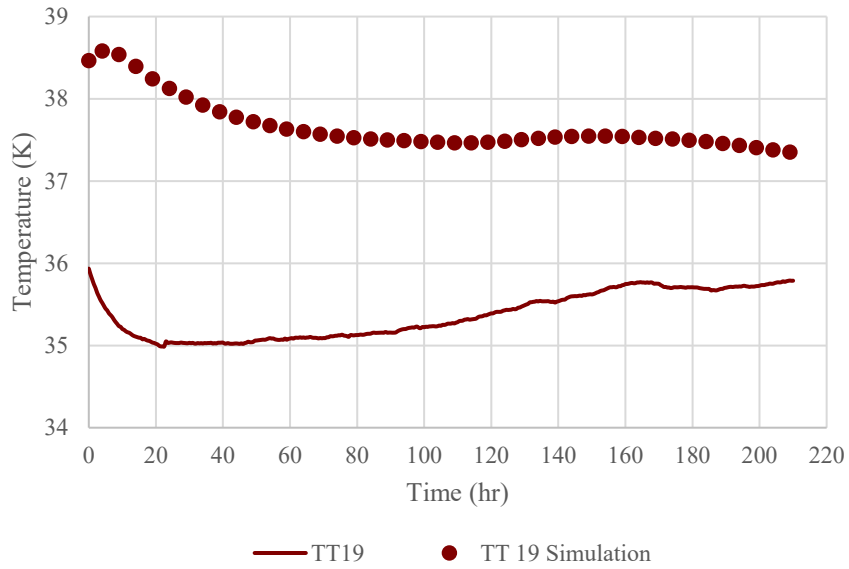
(a)



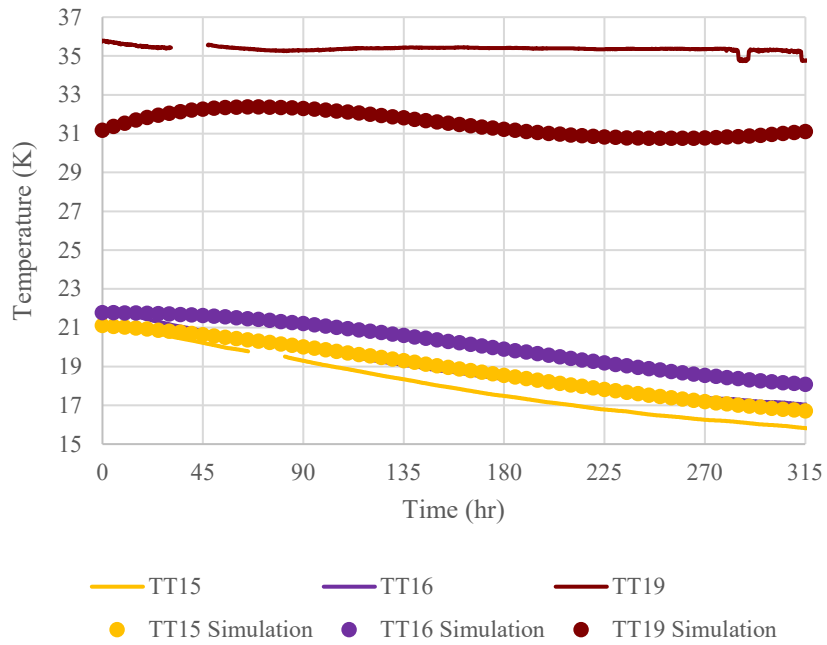
(b)

Fig. 10. Densification model liquid temperature comparison with experimental results (a)

100% fill, (b) 67% fill



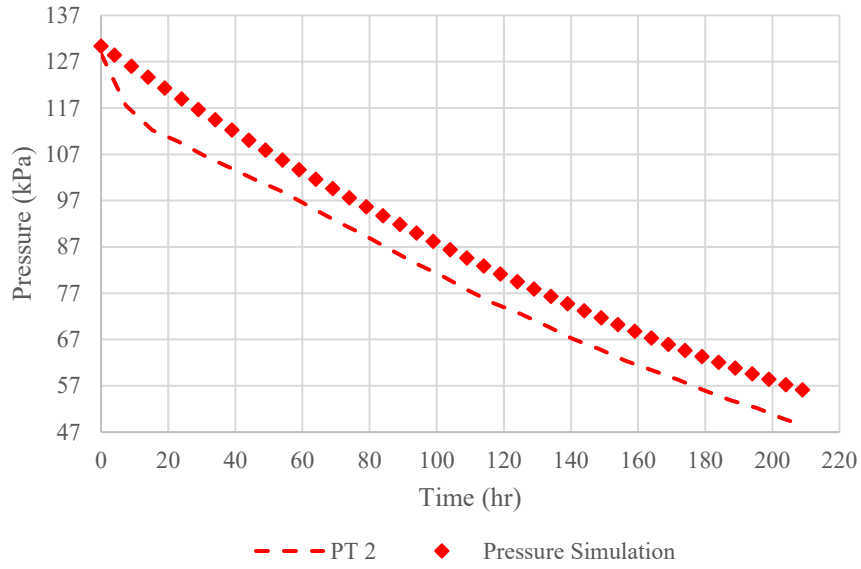
(a)



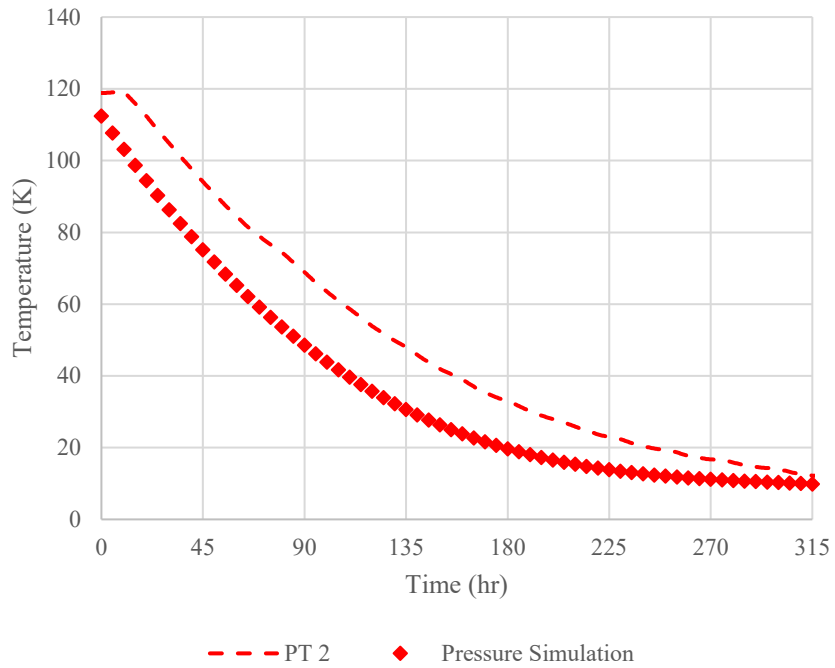
(b)

Fig. 11. Densification model ullage temperature comparison with experimental results (a)

100% fill, (b) 67% fill

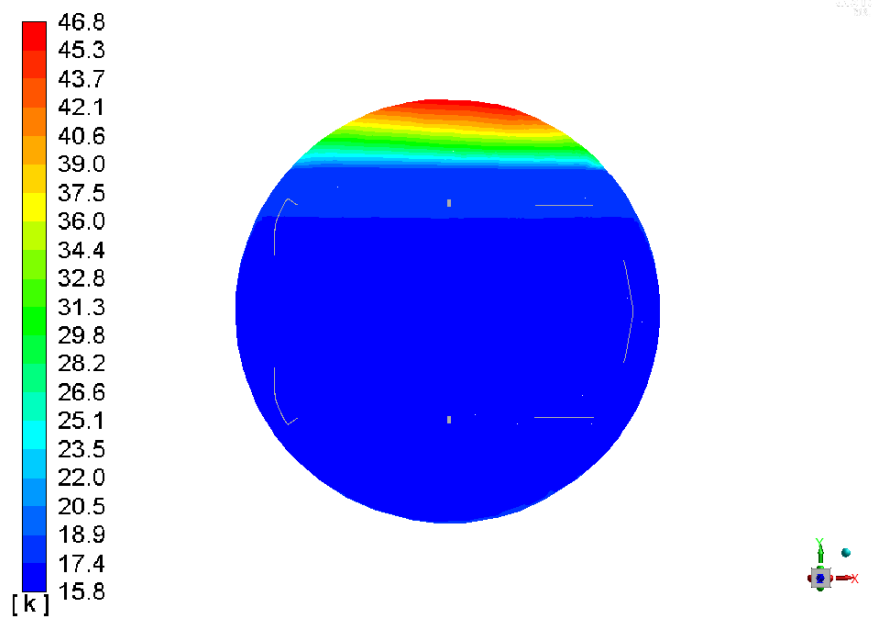


(a)

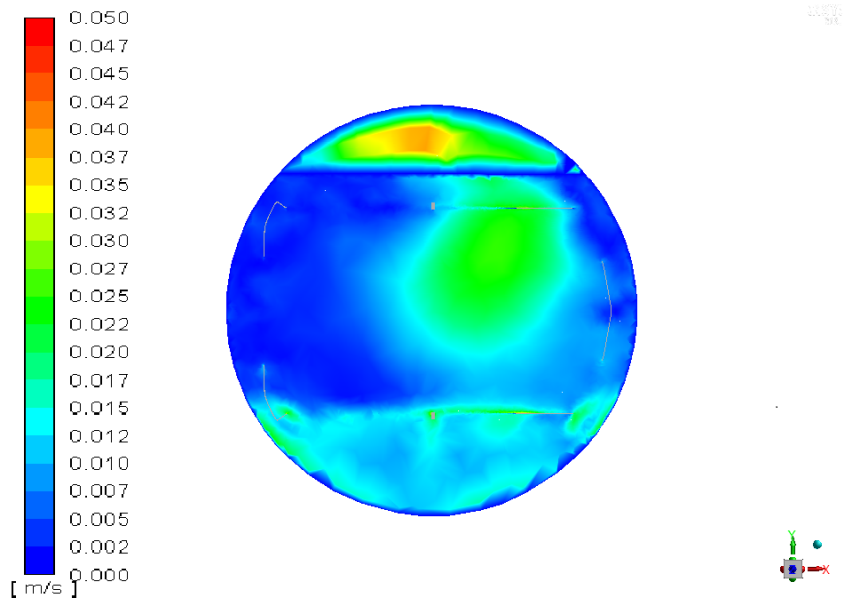


(b)

Fig. 12. Densification model pressure comparison with experimental results (a) 100% fill,
(b) 67% fill

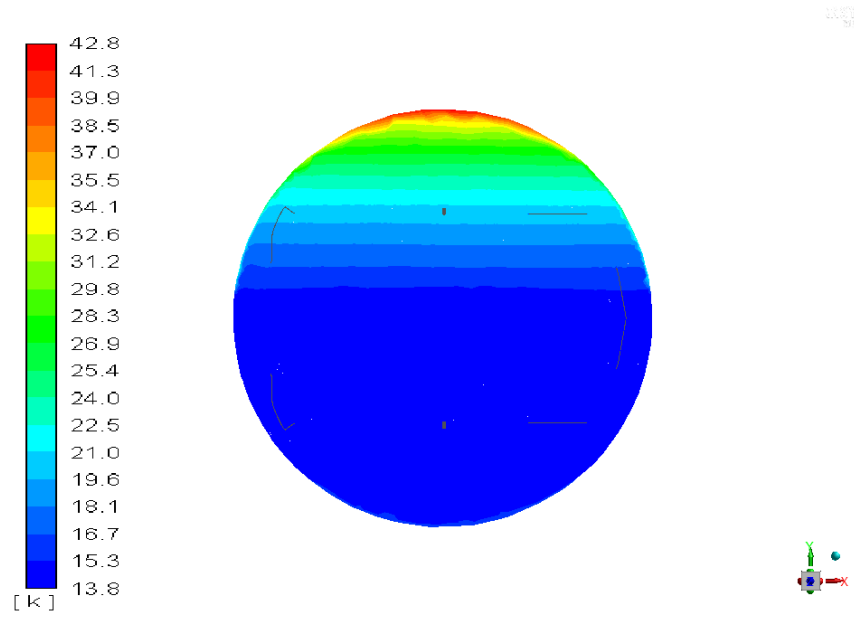


(a)

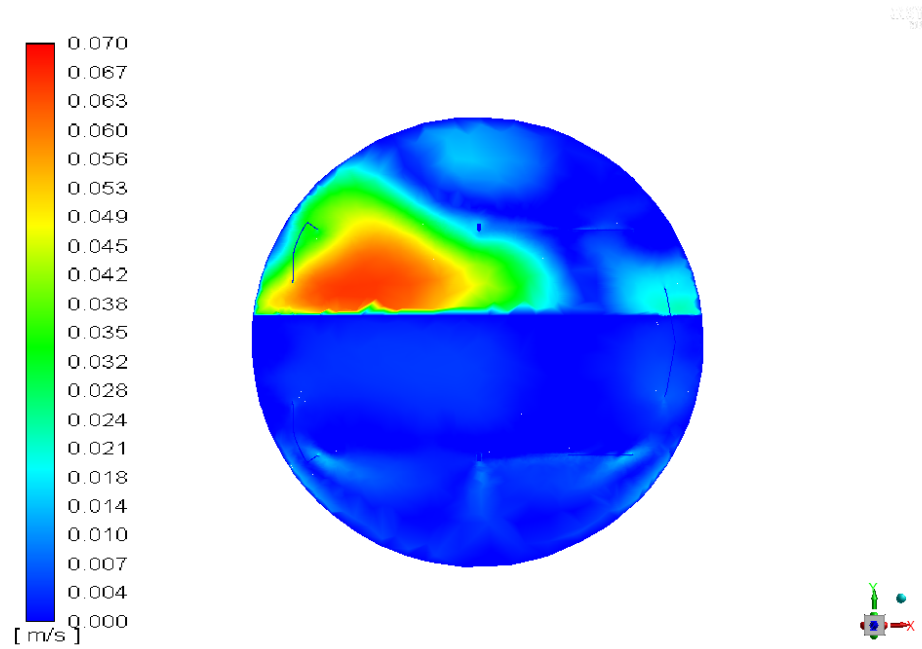


(b)

Fig. 13. Densification 100% fill at time=210 hours: (a) temperature profile, and (b) velocity profile



(a)



(b)

Fig. 14. Densification 67% fill at time=315 hours: (a) temperature profile, and (b) velocity profile

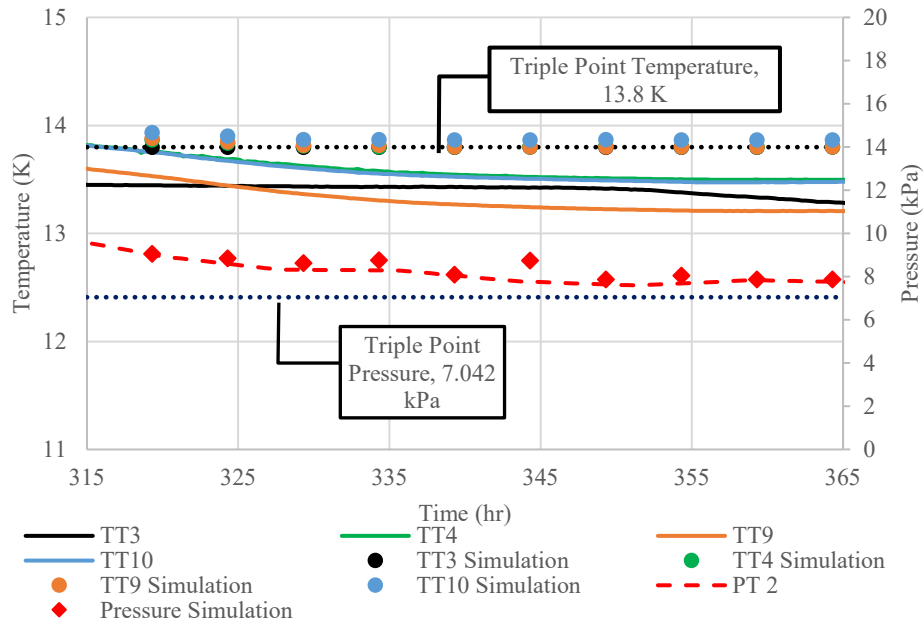
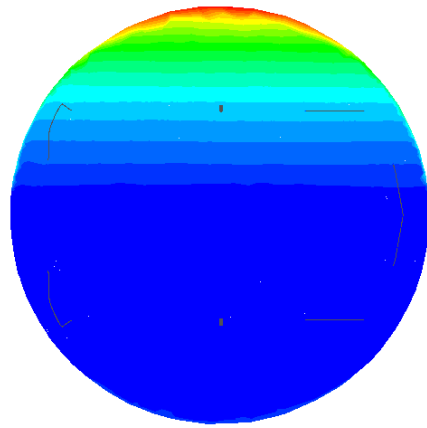
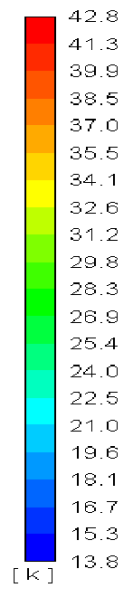
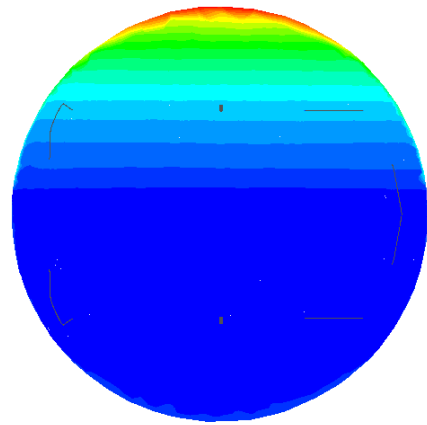
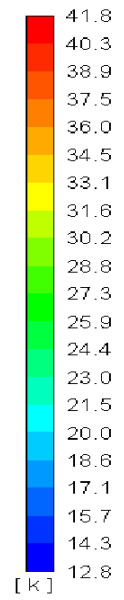


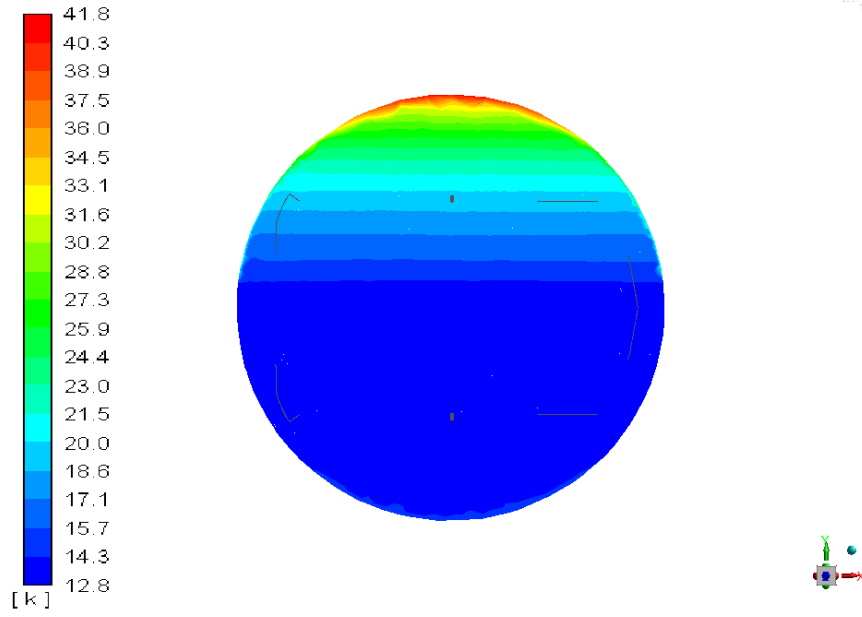
Fig. 15. 67% tank fill solidification experimental pressure and temperature compared to the simulation



(a)

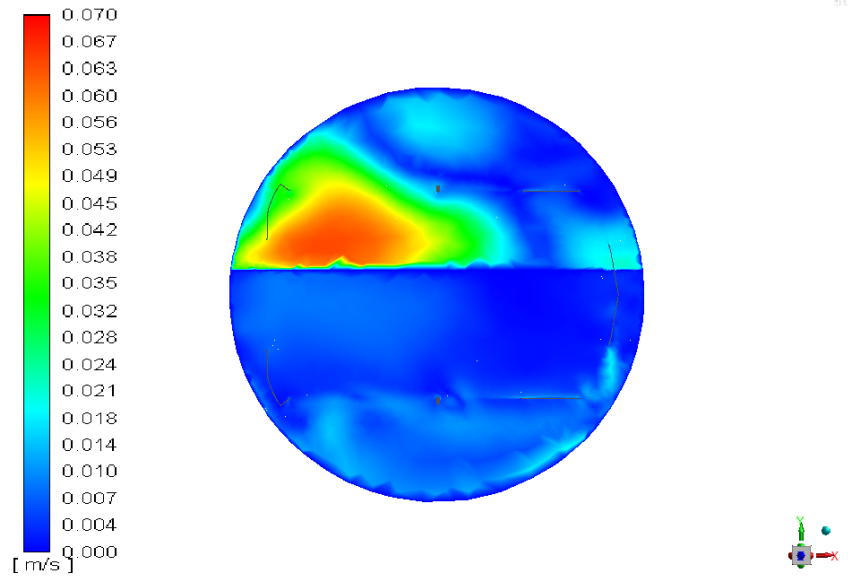


(b)

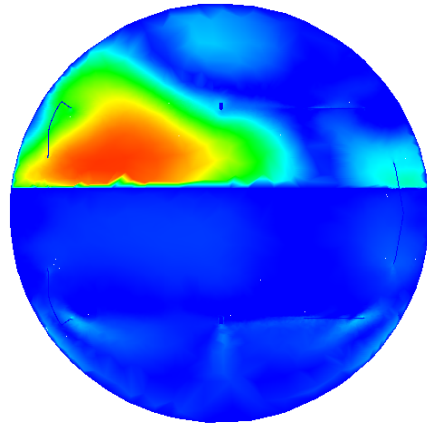
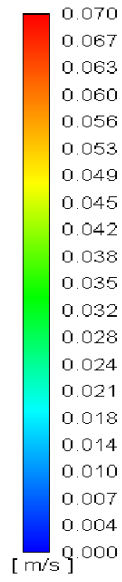


(c)

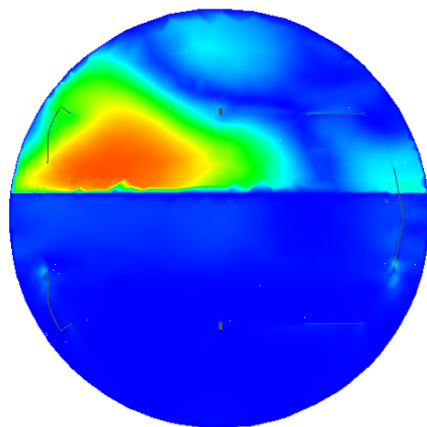
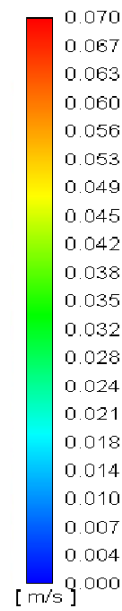
Fig. 16. Temperature: (a) onset of visible solidification, (b) 15 hours of solidification, (c) approximately 30 hours of solidification



(a)



(b)



(c)

Fig. 17. Velocity: (a) onset of visible solidification, (b) 15 hours of solidification, (c) approximately 50 hours of solidification

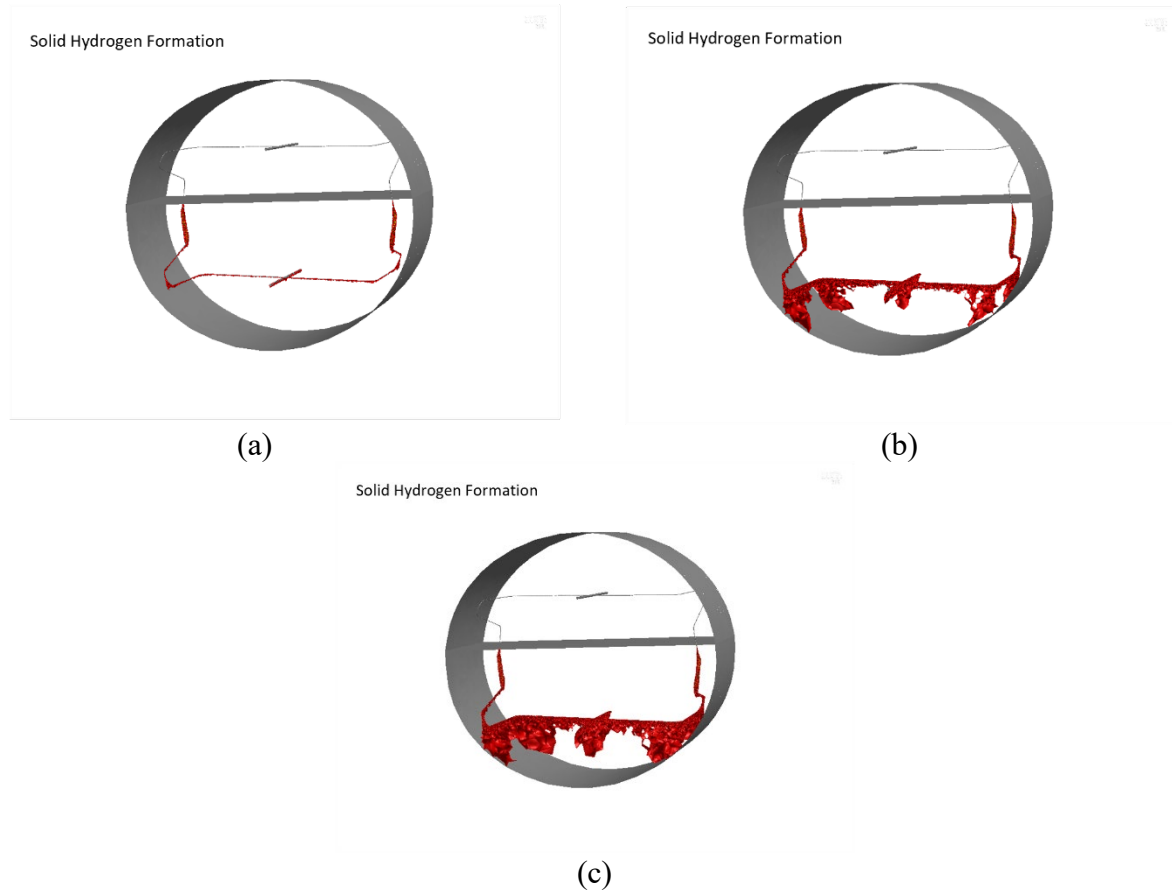


Fig. 18. Phase Front using a Solid Phase Fraction of 0.05 (shown in red): (a) onset of visible solidification, (b) 15 hours of solidification, (c) approximately 50 hours of solidification.

Table 1. Temperature sensor coordinates inside the GODU-LH2 IRAS tank

Sensor #	Distance (m)			Sensor #	Distance (m)		
	X-dir	Y-dir	Z-dir		X-dir	Y-dir	Z-dir
TT1	-4.11	0.57	0.16	TT11	-4.11	1.24	0.00
TT2	-4.11	0.57	-0.99	TT12	-4.11	1.24	1.27
TT3	0.12	0.57	0.08	TT13	-4.11	2.12	0.00
TT4	0.12	0.92	0.08	TT14	-4.11	1.85	0.08
TT5	6.27	0.57	0.00	TT15	0.12	1.85	0.08
TT6	6.27	0.57	1.15	TT16	0.12	2.12	0.08
TT7	6.27	1.24	0.16	TT17	6.27	2.12	0.00
TT8	6.27	1.24	-1.10	TT18	6.27	1.85	1.39
TT9	0.12	1.24	0.08	TT19	6.27	2.72	0.00

TT10	0.12	1.54	0.08	TT20	-4.11	2.72	0.00
------	------	------	------	------	-------	------	------

*Note: Directions correspond to the coordinate system in Fig 2

Table 2. GODU-LH2 boiloff heat leak results

Fill Level	Boiloff Flow Rate (slpm)	Tank Pressure (kPa)	Avg. Liquid Temp (K)	Avg. TT19 Reading (K)	Liquid Heat Load (W)	Ullage Heat Load (W)	Total Heat Load (W)	Total Heat Flux [†] (W/m ²)
67%	295	117.2	20.4	41.3	196	100	296	1.28
100%	351	109.6	20.3	34.5	234	81	315	1.36

[†]Based on log-mean area between the outside of the inner shell and the inside of the outer shell

Table 3. Maximum percent errors between simulation predictions and experimental results for three meshes

Steady-State					
100% fill level			67% fill level		
Mesh Cell Count	Maximum Percent Error in Pressure	Maximum Percent Error in Temperature, Diode	Mesh Cell Count	Maximum Percent Error in Pressure	Maximum Percent Error in Temperature, Diode
200k	0.8%	9.4%, TT19	320k	0.3%	14.6%, TT19
350k	0.7%	9.1%, TT19	430k	0.2%	12.0%, TT19
500k	0.7%	8.9%, TT19	660k	0.2%	9.5%, TT19
Densification					
100% fill level			67% fill level		
Mesh Cell Count	Maximum Percent Error in Pressure	Maximum Percent Error in Temperature, Diode	Mesh Cell Count	Maximum Percent Error in Pressure	Maximum Percent Error in Temperature, Diode
200k	9.8%	13.2%, TT19	320k	18.9%	11.4%, TT16
350k	6.5%	11.3%, TT19	430k	11.3%	10.7%, TT19
500k	4.8%	9.4%, TT19	660k	11.2%	7.8%, TT16
Solidification					
67% fill level					
Mesh Cell Count	Maximum Percent Error in Pressure, Transducer		Maximum Percent Error in Temperature, Diode		
320k	18.1%		11.6%, TT16		
430k	14.0%		9.3%, TT19		
660k	9.5%		7.2%, TT16		